

Supporting Information

Diketopyrrolopyrrole-based Small Molecules for Solution-Processed n- Channel Organic Thin Film Transistors

Qian Zhou,^a Yu Jiang,^a Tian Du,^a Zhongli Wang,^a Ziqi Liang,^a Yang Han,^{*a} Yunfeng Deng,^a

Hongkun Tian,^{*b} Yanhou Geng^{*ac}

^aSchool of Materials Science and Engineering and Tianjin Key Laboratory of Molecular Optoelectronic Science, Tianjin University, Tianjin 300072, P. R. China.

^bState Key Laboratory of Polymer Physics and Chemistry, Changchun Institute of Applied Chemistry, Chinese Academy of Sciences, Changchun, 130022, P. R. China.

^cJoint School of National University of Singapore and Tianjin University, International Campus of Tianjin University, Binhai New City, Fuzhou 350207, China.

*E-mail: yang.han@tju.edu.cn; hktian@ciac.ac.cn; yanhou.geng@tju.edu.cn

1. Instruments, OTFTs fabrication and measurements	S-3
2. Synthetic procedures	S-6
3. ^1H and ^{13}C NMR spectra	S-8
4. MALDI-TOF mass spectra	S-12
5. Thermal properties	S-14
6. X-ray crystallography	S-15
7. Density functional theory calculations of DPP1012-4F and DPP1012-4Cl	S-16
8. OTFT performances	S-17
9. The molecular packing diagram in annealed films	S-19
10. References	S-19

1. Instruments, OTFTs fabrication and measurements

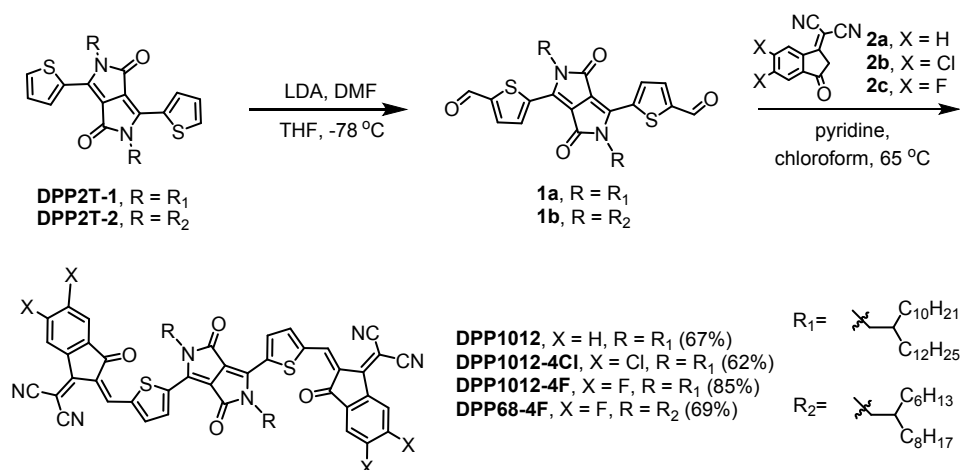
Instruments. ^1H NMR (25 °C, CDCl_3 with tetramethylsilane as internal standard) and ^{13}C NMR (120 °C, 1,1,2,2-tetrachloroethane- d_2) spectra of all new compounds were measured by a Bruker AV 400-MHz spectrometer. Matrix-assisted laser desorption ionization time-of-flight (MALDI-TOF) mass spectra was recorded on a Bruker/AutoflexIII Smartbean MALDI mass spectrometer with 2-[(2E)-3-(4-*tert*-butylphenyl)-2-methylprop-2-enylidene] malononitrile (DCTB) as the matrix in a reflection mode. Elemental analysis was measured by a FlashEA1112 elemental analyzer. Thermogravimetric analysis (TGA) was carried out on a TA Q50 thermogravimetric analyzer with the heating rate of 10 °C min^{-1} at a nitrogen flow. Differential scanning calorimetry (DSC) was conducted on a TA Q2000 instrument with a heating/cooling rate of 10 °C min^{-1} under nitrogen. Needle-like single crystals of **DPP68-4F** were obtained by slow diffusion of methanol into its dilute toluene solution at room temperature. The data were collected on a “Bruker APEX-II CCD” diffractometer. In the Olex2, the structure was solved with the ShelXT structure solution program using Intrinsic Phasing and refined with the ShelXL refinement package using Least Squares minimisation. UV-*vis*-NIR absorption spectra of solutions (10^{-5} mol L^{-1} in chloroform) and thin films (prepared by spin-coating 5.0 mg mL^{-1} CHCl_3 solutions on quartz substrates) of compounds were recorded on a Shimadzu UV3600-plus spectrometer. Cyclic voltamograms (CV, scan rate: 100 mV s^{-1}) were measured using a CHI660 electrochemical analyzer with a three-electrode cell with tetrabutylammonium hexafluorophosphate (Bu_4NPF_6 , 0.1 mol L^{-1}) as the supporting electrolyte in anhydrous chloroform solutions. A Pt disk with 2 mm diameter, a

Pt wire and a saturated calomel electrode (SCE) were used as working, counter and reference electrodes, respectively. For calibration, the redox potential of ferrocene/ferrocenium (Fc/Fc⁺) was measured under the same conditions, which was 0.41 eV versus SCE. The highest occupied molecular orbital (HOMO) and the lowest unoccupied molecular orbital (LUMO) energy levels were calculated according to the equations $E_{\text{HOMO}} = -(4.80 + E_{\text{onset ox}})$ eV and $E_{\text{LUMO}} = -(4.80 + E_{\text{onset re}})$ eV, in which $E_{\text{onset ox}}$ and $E_{\text{onset re}}$ represent reduction and oxidation onsets, respectively. Density functional theory (DFT) calculation was carried out using Gaussian 09 with a hybrid B3LYP correlation functional and 6-31G (d) basis set. All alkyl substituents were replaced with methyl groups in order to simplify the calculations. Atomic force microscopy (AFM) measurements were carried out in tapping mode on a Bruker MultiMode 8 atomic force microscope. In-plane and Out-of-plane X-ray diffraction (XRD) were conducted on a Rigaku Smart Lab with Cu K $_{\alpha}$ source ($\lambda = 1.54056 \text{ \AA}$).

OTFT fabrication and measurements. The charge transport properties of the molecules were characterized by using top gate/bottom contact (TG/BC) OTFTs. Highly n-doped silicon wafers covered with a 300 nm thick thermally grown SiO₂ layer, which are commercially available and have flat and smooth surface, were used as substrates. The substrates were washed by an ultrasonic cleaner with deionized water, acetone and isopropanol, respectively and then dried under a nitrogen flow and heated at 120 °C for 10 min. Au (~30 nm) was deposited on the silicon substrate as source and drain electrodes with shadow mask of W/L = 112 (W = 5600 μm , L = 50 μm). Subsequently, the semiconductor films were

prepared by spin-coating from respective hot solutions (70 °C chlorobenzene solutions for **DPP1012-4F** and **DPP68-4F**, 100 °C *o*-xylene solutions for **DPP1012** and **DPP1012-4Cl**) with a concentration of 5.0 mg mL⁻¹ at 1000 rpm for 90 s. The films were treated without and with thermal annealing for 10 min. CYTOP (Asahi Glass, type CTL-809M) as the gate dielectric was spin-cast at 2000 rpm for 120 s and annealed at 100 °C for 40 min. Finally, Al (~80 nm) was vacuum-evaporated as the device gate. All the device fabrication procedures were conducted in a glove box. OTFT devices were measured in a glove box with Keysight B1500A analyzer. Field-effect mobility in saturation regime was calculated by using the equation: $I_{\text{sat DS}} = (\mu C_i W / 2L)(V_{\text{GS}} - V_{\text{th}})^2$, in which I_{DS} is the drain-source current, μ is the field effect mobility, C_i (2.1 nF cm⁻²) is the capacitance per unit area of the dielectric layer, V_{GS} and V_{th} are the gate voltage and threshold voltage, respectively.

2. Synthetic procedures



Scheme S1. Chemical structures and synthesis of **DPP1012**, **DPP1012-4Cl**, **DPP1012-4F** and **DPP68-4F**.

The compounds **DPP2T-1** and **DPP2T-2** were prepared according to the previous report.¹

Synthesis of 1a.² To a solution of diisopropylamine (0.61 mL, 4.32 mmol) and THF (30 mL) in 100 mL schlenk flask was added n-BuLi (1.6 M in hexane, 1.80 mL, 2.88 mmol) dropwise before stirring at 0 °C for 1 h to prepare fresh lithium diisopropylamide (LDA). Compound **DPP2T-1** (0.70 g, 0.72 mmol) in THF (10 mL) was then added dropwise into the flask at -78 °C. After stirring at -78 °C for 1 h, dry DMF (0.55 mL, 7.19 mmol) was added dropwise at -78 °C. The mixture was allowed to warm up to room temperature and stirred for 2 h. Then the mixture was quenched with 5.0 mL of water. The aqueous layer was extracted with dichloromethane (3 × 50 mL). The combined extracts were washed with distilled water and dried over anhydrous MgSO₄. After removal of the solvents under reduced pressure, the residue was purified by chromatography with silica (eluent: petroleum ether/ethyl acetate =

20/1 to 10/1) to afford **1a** as a dark red solid (0.48 g, yield: 65%). ^1H NMR (CDCl_3 , 400 MHz, ppm): δ 10.03 (s, 2H), 9.02-9.03 (d, $J = 4.4$ Hz, 2H), 7.86-7.87 (d, $J = 4.0$ Hz, 2H), 4.03-4.05 (d, $J = 7.6$ Hz, 4H), 1.80-1.95 (m, 2H), 1.12-1.40 (m, 80H), 0.81-0.95 (m, 12H).

Synthesis of 1b. **1b** (0.99 g, yield: 62%) was synthesized using similar synthetic procedure as **1a**, starting from **DPP2T-2** (1.50 g, 2.00 mmol), diisopropylamine (1.69 mL, 12.01 mmol), *n*-BuLi (1.6 M in hexane, 5.01 mL, 8.01 mmol), DMF (1.54 mL, 20.02 mmol) and THF (110 mL). ^1H NMR (CDCl_3 , 400 MHz, ppm): δ 10.03 (s, 2H), 9.02-9.03 (d, $J = 4.0$ Hz, 2H), 7.87-7.88 (d, $J = 4.0$ Hz, 2H), 4.04-4.05 (d, $J = 7.6$ Hz, 4H), 1.80-1.96 (m, 2H), 1.10-1.45 (m, 48H), 0.75-0.95 (m, 12H).

3. ^1H and ^{13}C NMR spectra

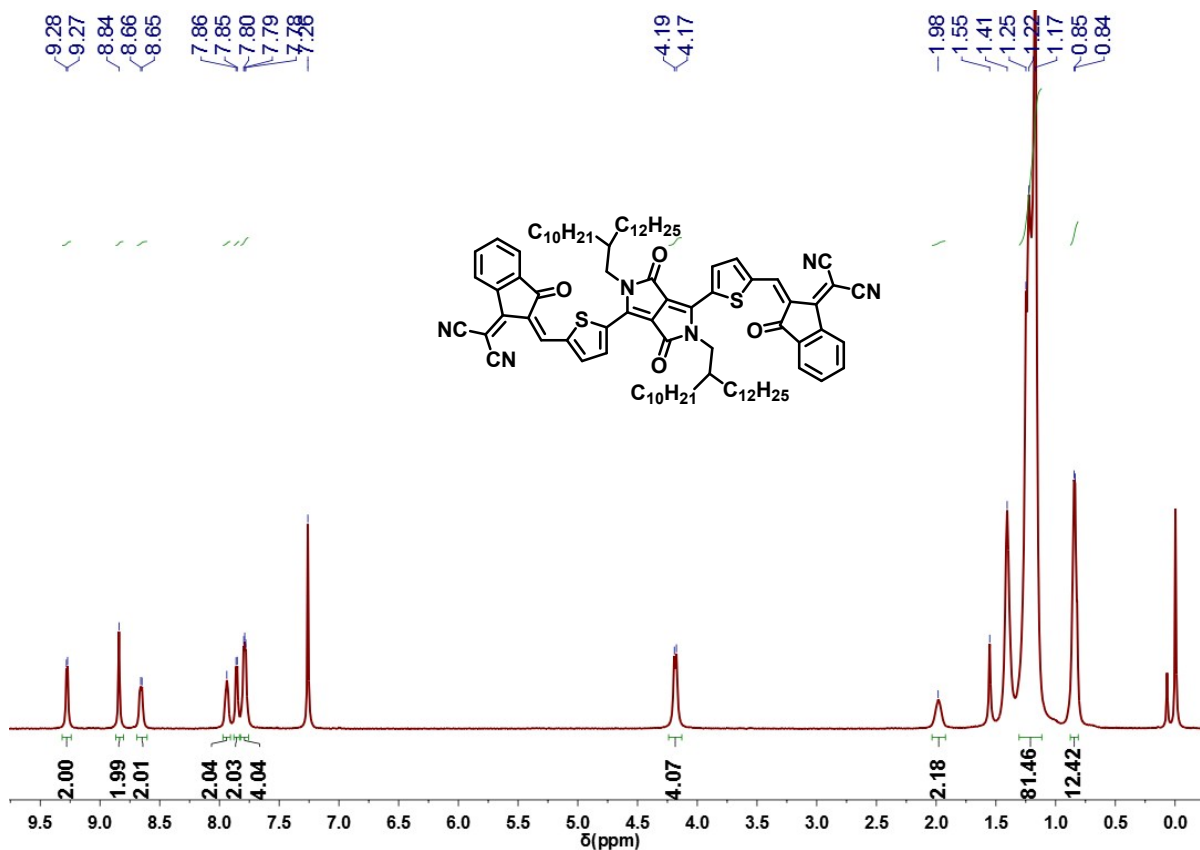


Figure S1. ^1H NMR spectrum of DPP1012.

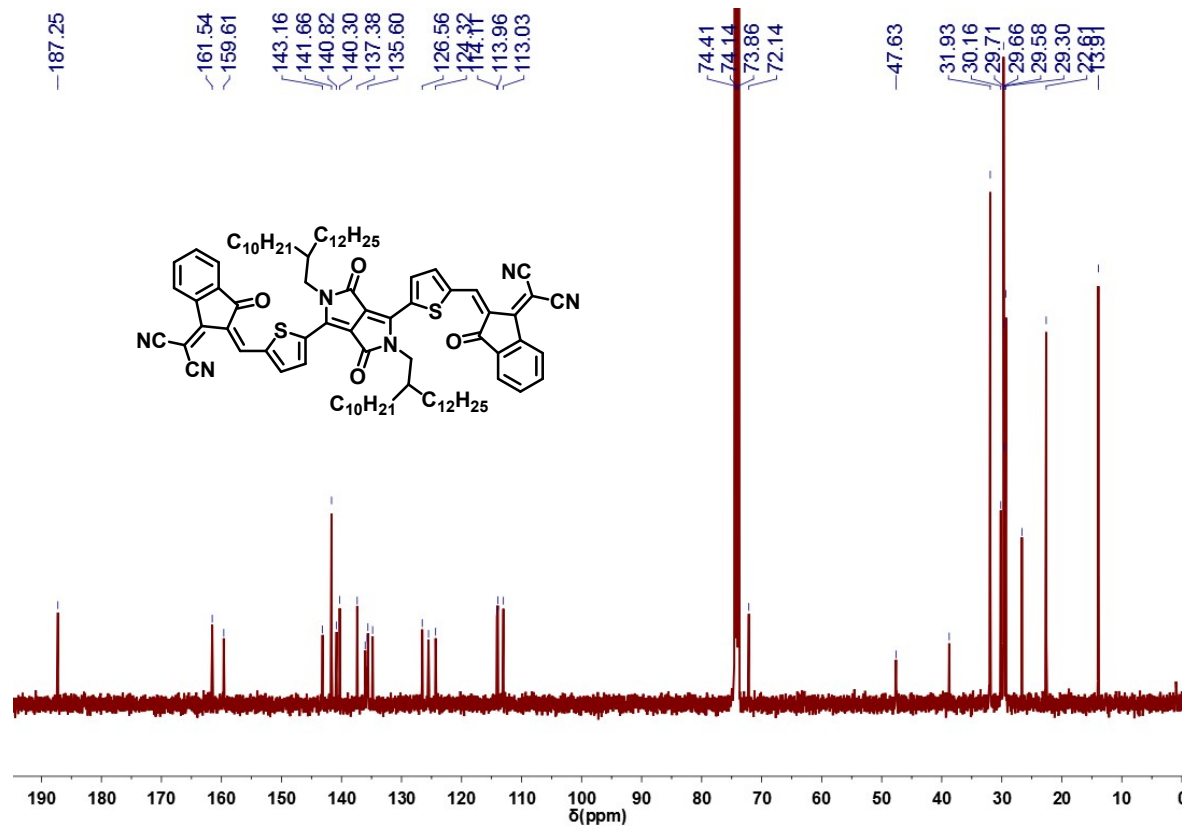


Figure S2. ^{13}C NMR spectrum of DPP1012.

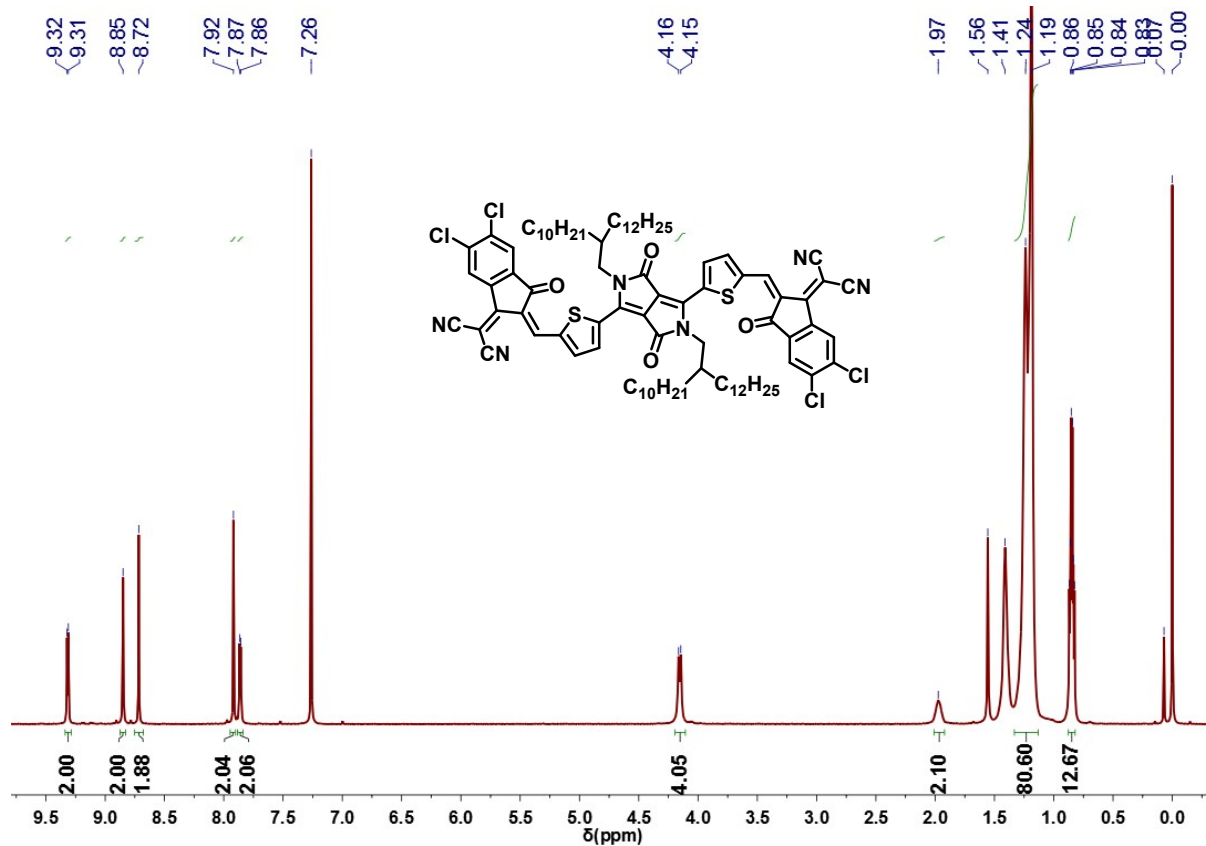


Figure S3. ¹H NMR spectrum of DPP1012-4Cl.

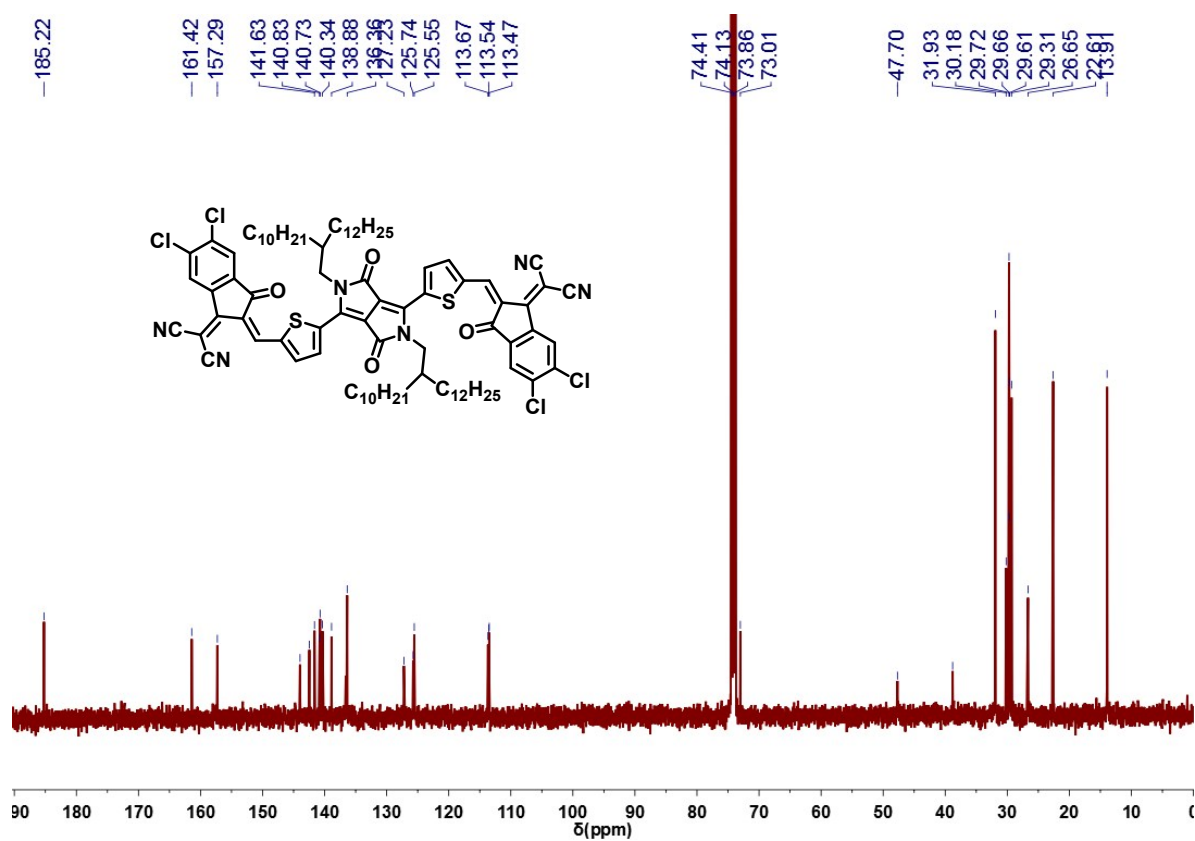


Figure S4. ¹³C NMR spectrum of DPP1012-4Cl.

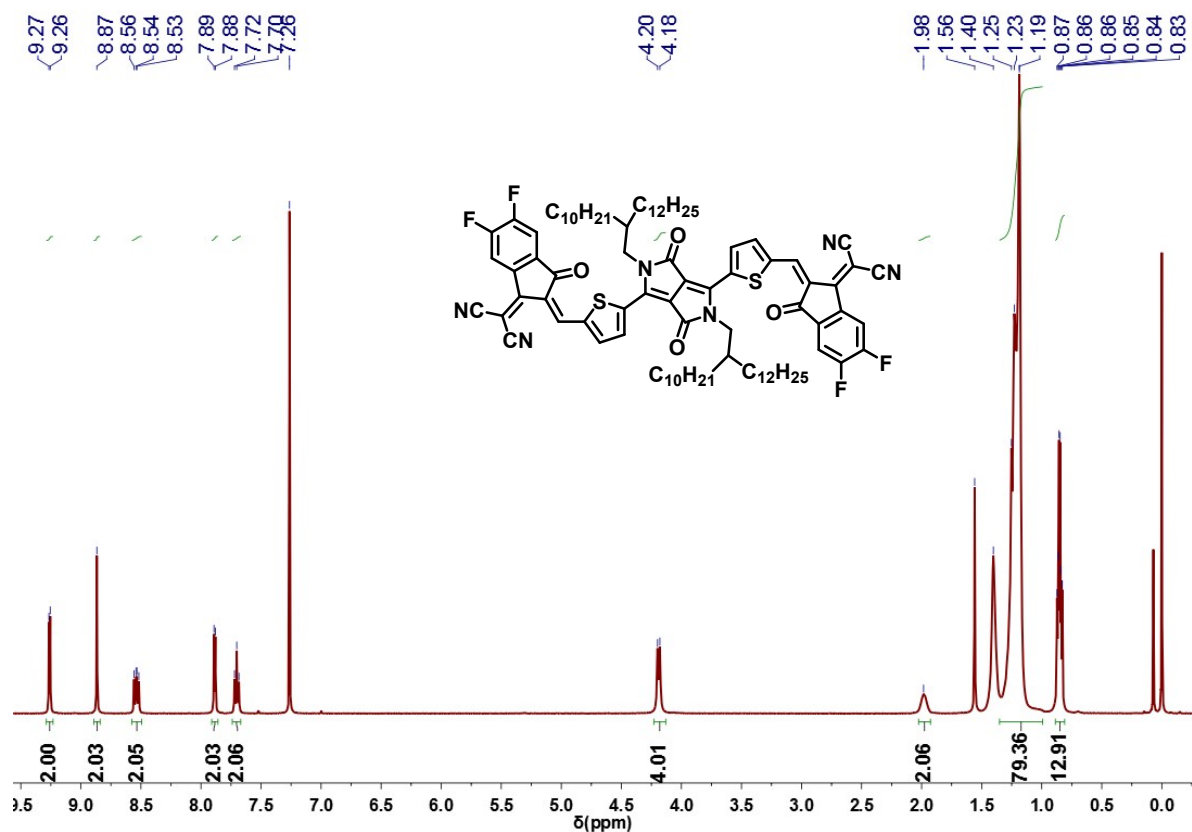


Figure S5. ¹H NMR spectrum of DPP1012-4F.

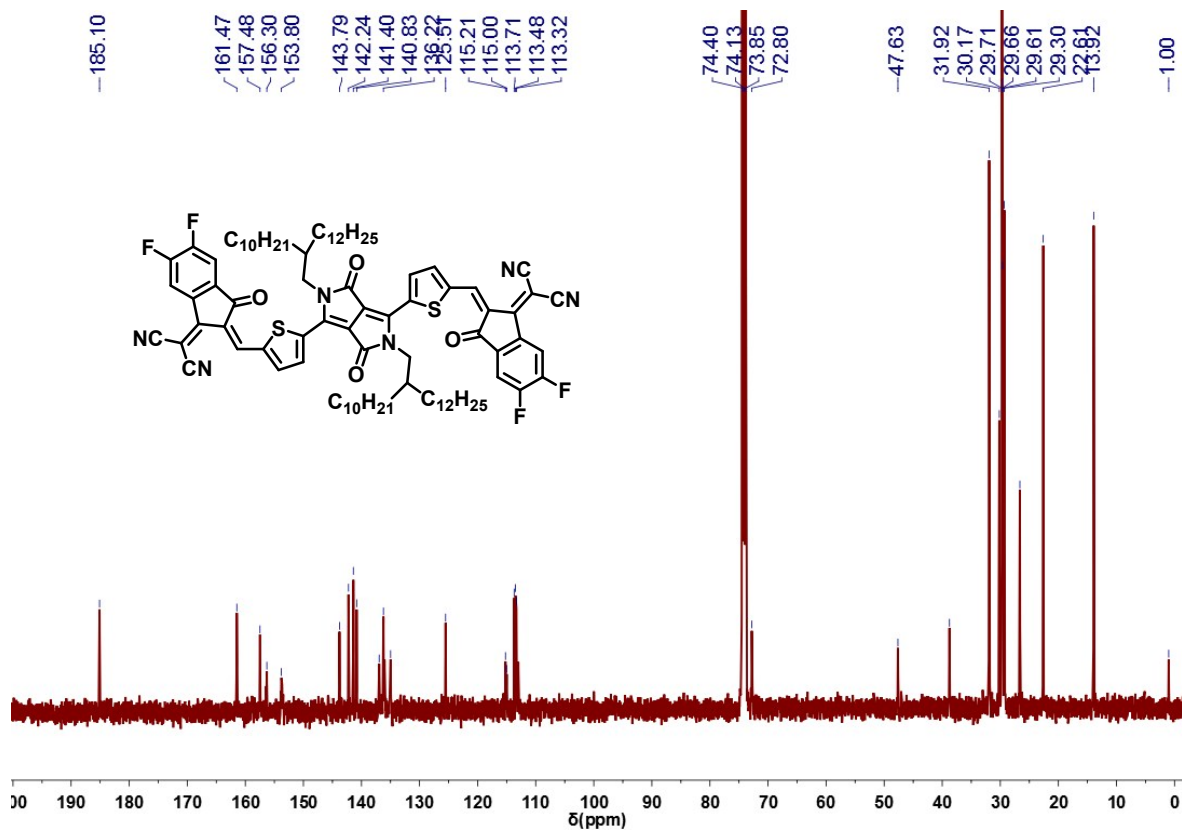


Figure S6. ¹³C NMR spectrum of DPP1012-4F.

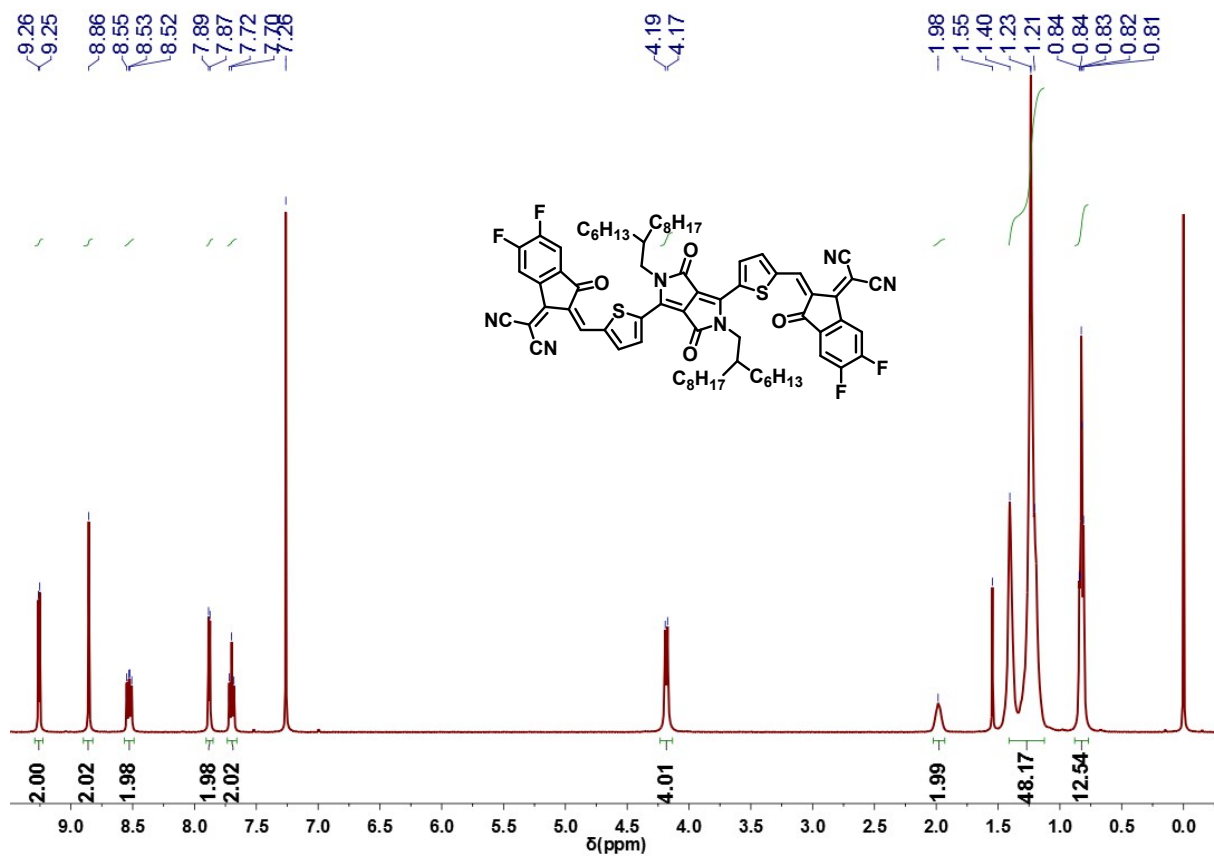


Figure S7. ¹H NMR spectrum of DPP68-4F.

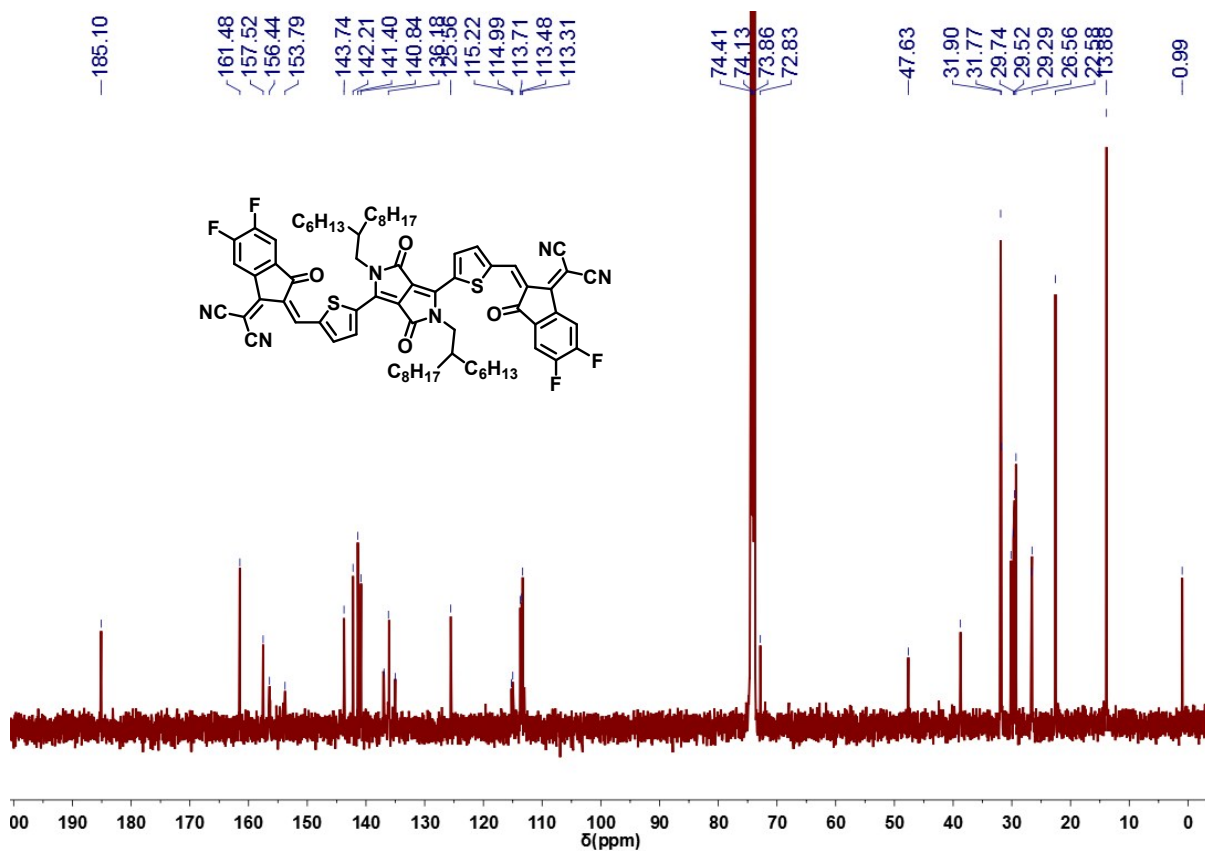


Figure S8. ¹³C NMR spectrum of DPP68-4F.

4. MALDI-TOF mass spectra

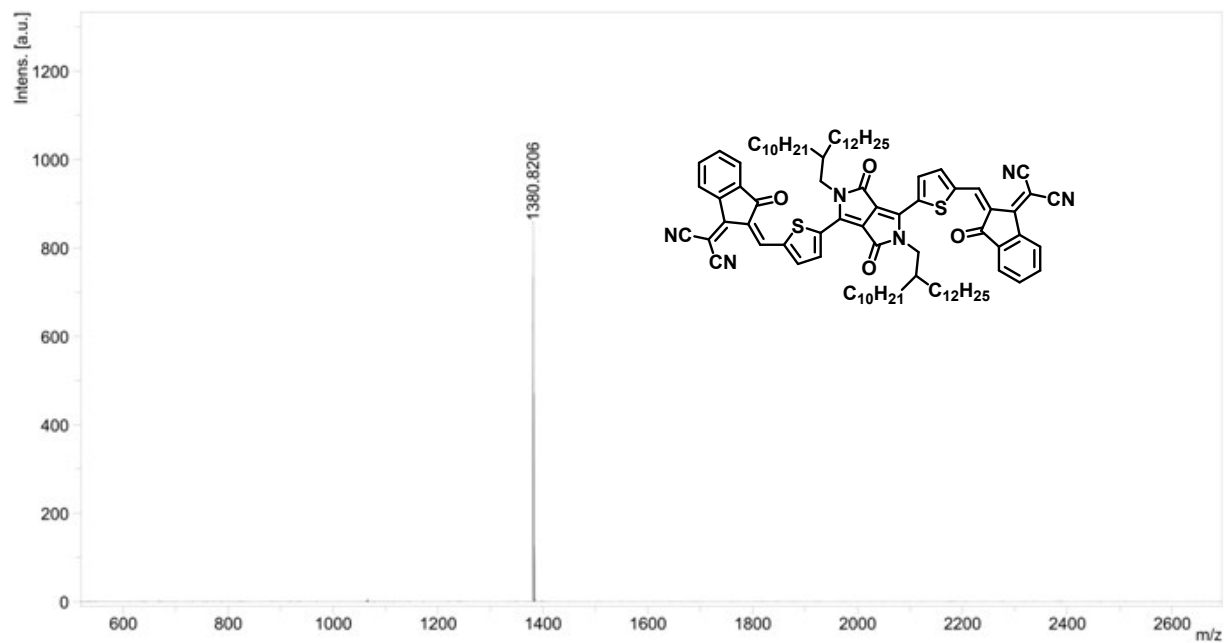


Figure S9. The MALDI-TOF mass spectrum of **DPP1012**.

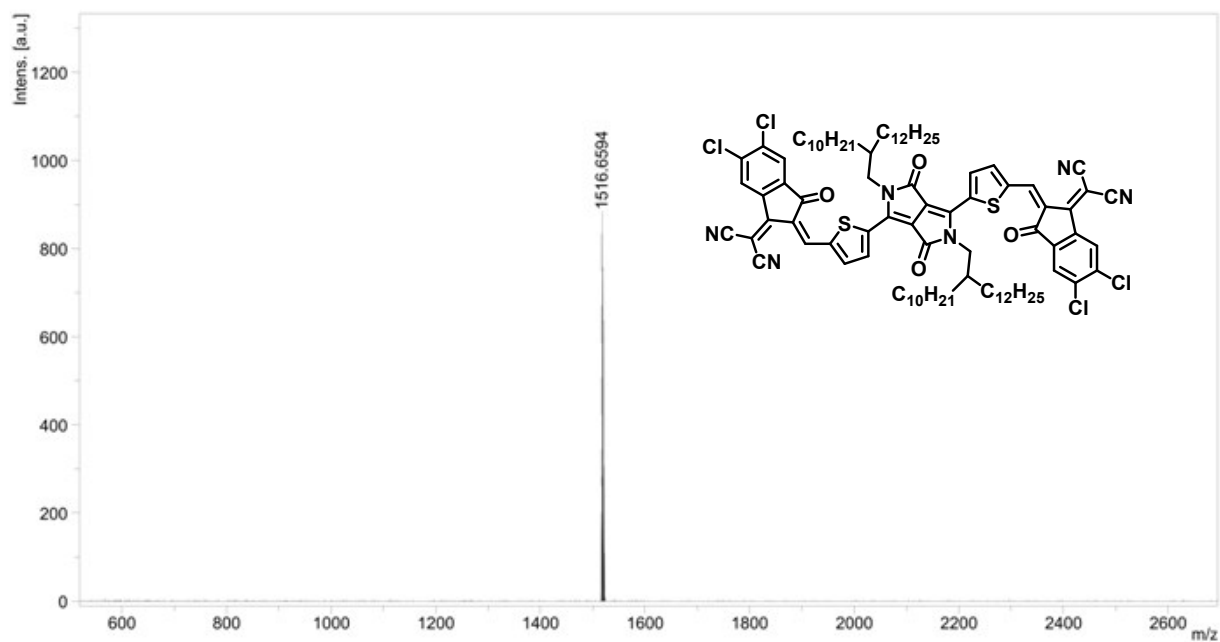


Figure S10. The MALDI-TOF mass spectrum of **DPP1012-4Cl**.

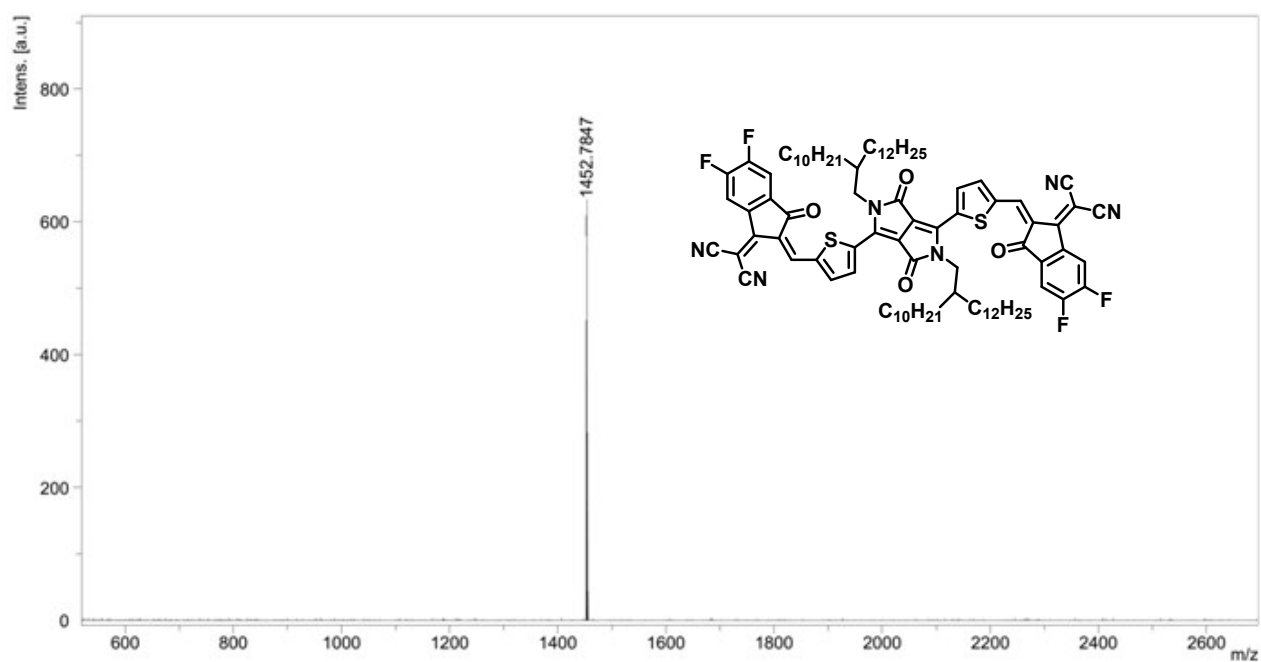


Figure S11. The MALDI-TOF mass spectrum of DPP1012-4F.

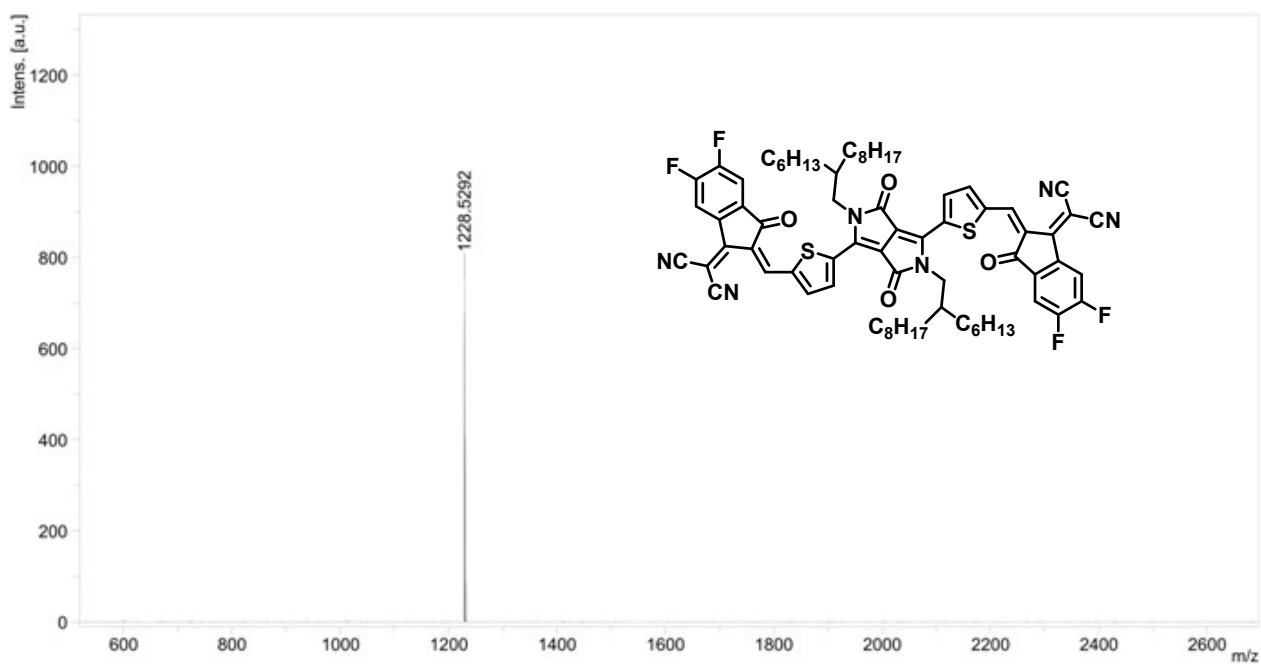


Figure S12. The MALDI-TOF mass spectrum of DPP68-4F.

5. Thermal properties

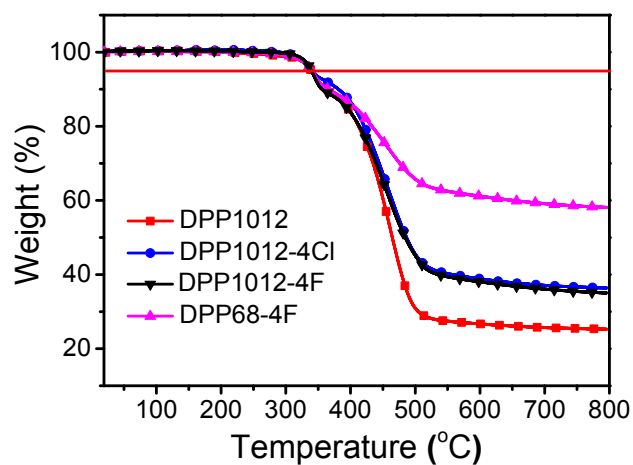


Figure S13. TGA curves of four compounds in N_2 with a heating rate of $10\text{ }^\circ\text{C}/\text{min}$.

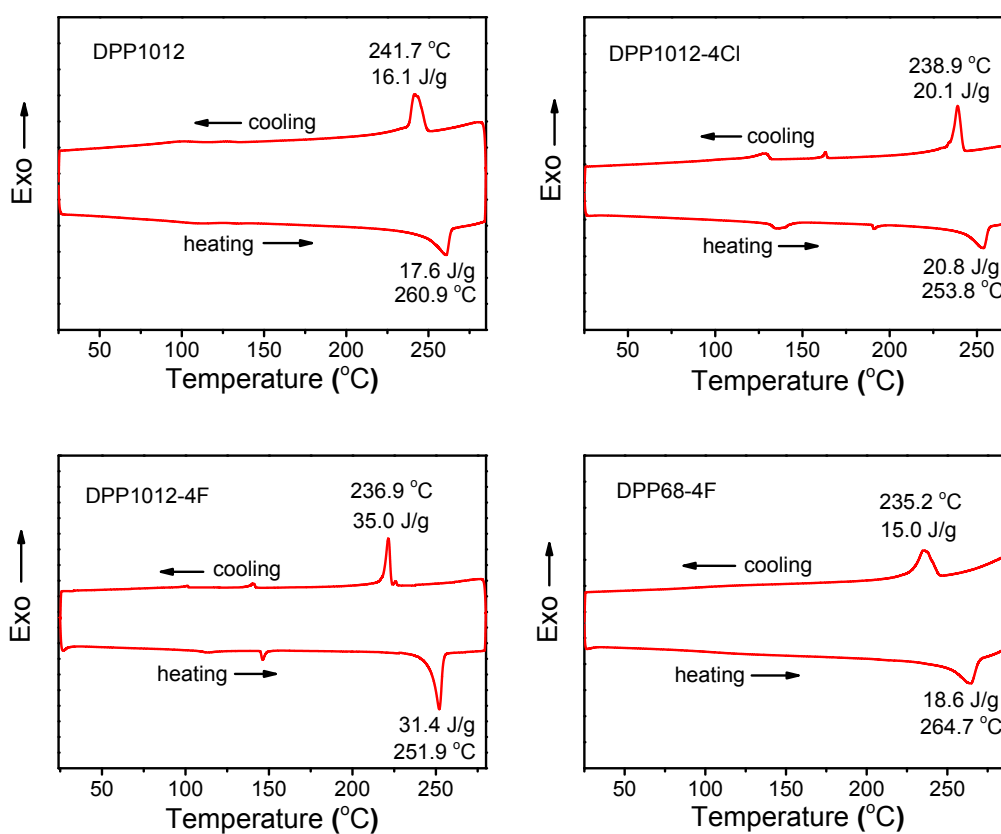


Figure S14. The first cooling and the second heating DSC curves of four compounds in N_2 with a heating/cooling rate of $10\text{ }^\circ\text{C}/\text{min}$.

6. X-ray crystallography

Table S1. Crystal data and structure refinement for **DPP68-4F**.

Identification code	DPP68-4F	
Empirical formula	C ₇₂ H ₇₆ F ₄ N ₆ O ₄ S ₂	
Formula weight	1229.50	
Temperature	170.01 K	
Wavelength	1.34139 Å	
Crystal system	Triclinic	
Space group	P-1	
Unit cell dimensions	a = 6.6078(7) Å	α = 96.078(4)°.
	b = 14.9482(15) Å	β = 95.431(5)°.
	c = 16.8745(18) Å	γ = 102.535(4)°.
Volume	1606.0(3) Å ³	
Z	1	
Density (calculated)	1.271 Mg/m ³	
Absorption coefficient	0.834 mm ⁻¹	
F(000)	650	
Crystal size	0.1 x 0.01 x 0.005 mm ³	
Theta range for data collection	3.741 to 54.959°.	
Index ranges	-8<=h<=7, -17<=k<=18, -19<=l<=20	
Reflections collected	15682	
Independent reflections	6045 [R(int) = 0.0427]	
Completeness to theta = 53.594°	99.1 %	
Absorption correction	Semi-empirical from equivalents	
Max. and min. transmission	0.7508 and 0.5458	
Refinement method	Full-matrix least-squares on F ²	
Data / restraints / parameters	6045 / 73 / 399	
Goodness-of-fit on F ²	1.045	
Final R indices [I>2σ(I)]	R1 = 0.0732, wR2 = 0.2127	
R indices (all data)	R1 = 0.1078, wR2 = 0.2450	
Extinction coefficient	n/a	
Largest diff. peak and hole	0.884 and -0.557 e.Å ⁻³	

7. Density functional theory calculations of DPP1012-4F and DPP1012-4Cl

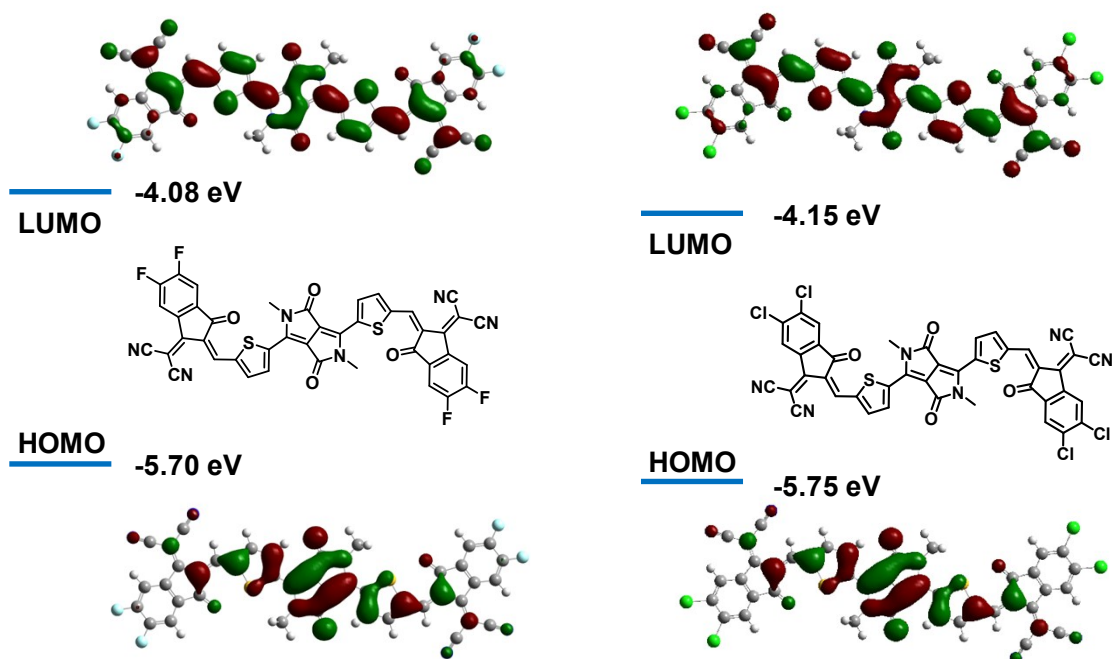


Figure S15. FMO distributions diagram of **DPP1012-4F** and **DPP1012-4Cl**. The branched alkyl chains were replaced with methyl groups in the calculations.

8. OTFT performances

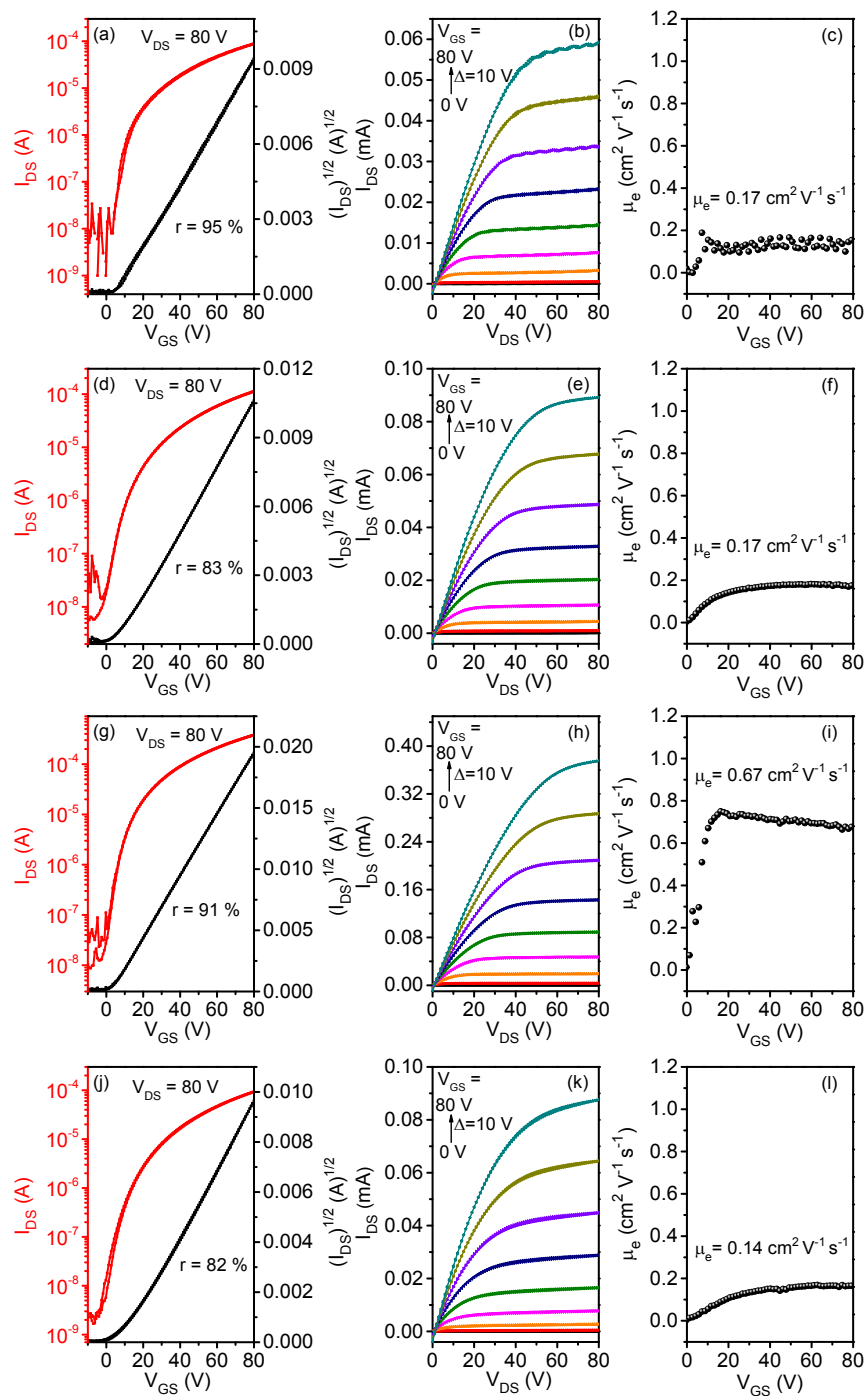


Figure S16. Typical transfer (a, d, g, j) and output (b, e, h, k) curves and μ_e versus V_G curves (c, f, i, l) of OTFTs based on as cast thin films of **DPP1012** (a-c), **DPP1012-4Cl** (d-f), **DPP1012-4F** (g-i) and **DPP68-4F** (j-l), and all devices were measured in glove box. Insets of (a), (d), (g) and (j) show the mobility reliability factors (r).

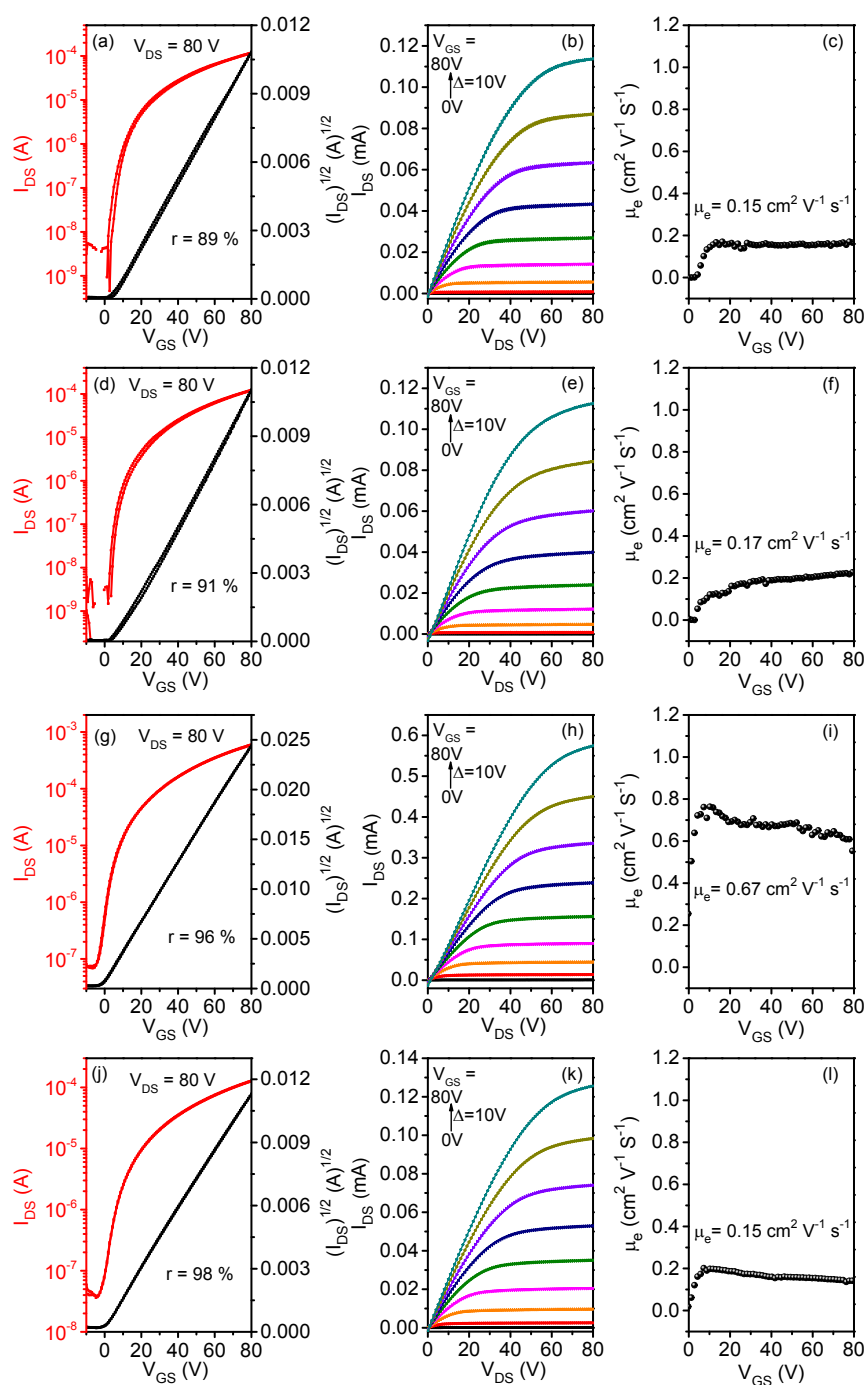


Figure S17. Typical transfer (a, d, g, j) and output (b, e, h, k) curves and μ_e versus VG curves (c, f, i, l) of OTFTs based on as cast thin films of **DPP1012** (a-c), **DPP1012-4Cl** (d-f), **DPP1012-4F** (g-i) and **DPP68-4F** (j-l). and all devices were measured in air. Insets of (a), (d), (g) and (j) show the mobility reliability factors (r).

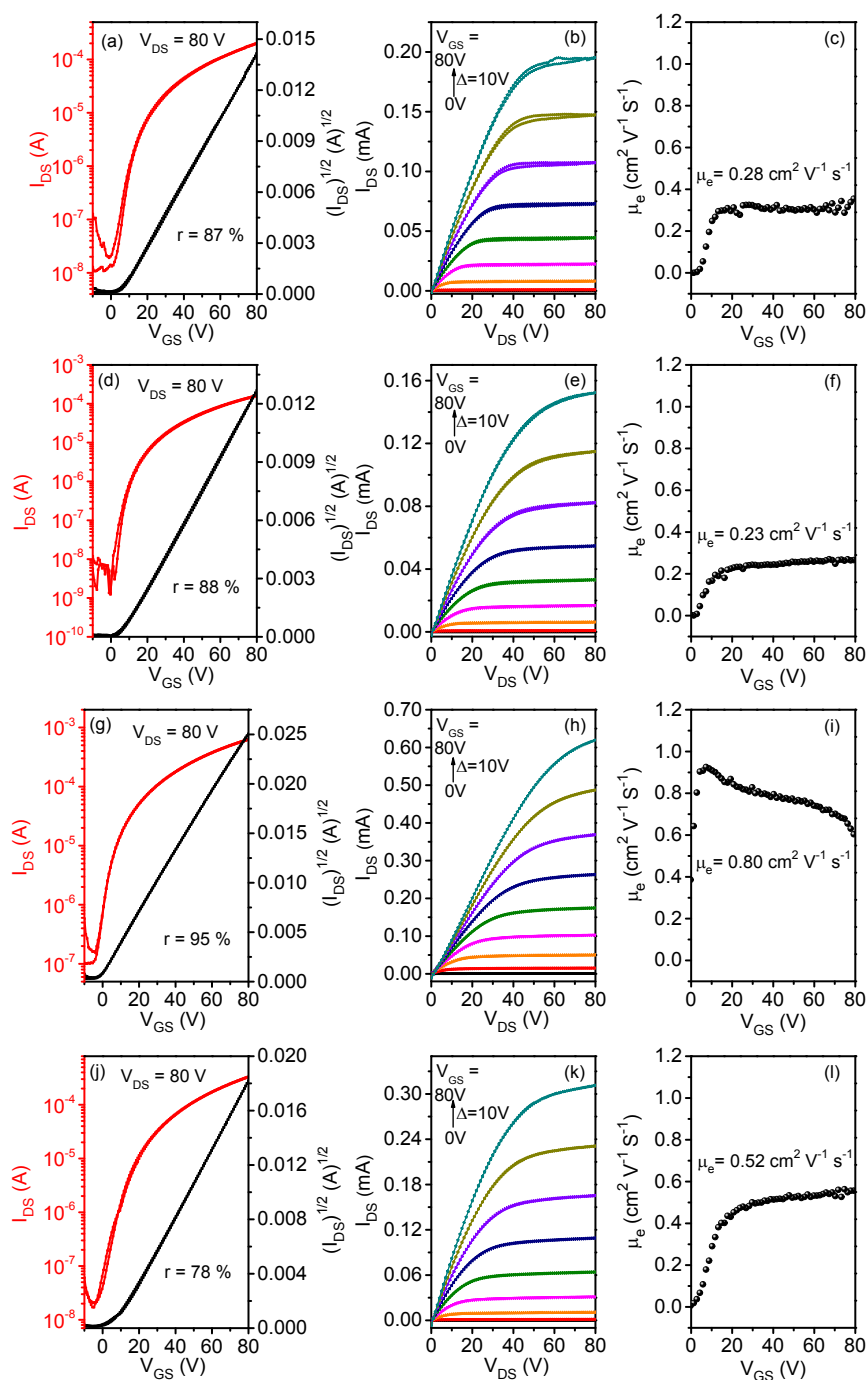


Figure S18. Typical transfer (a, d, g, j) and output (b, e, h, k) curves and μ_e versus V_G curves (c, f, i, l) of OTFTs based on thermally annealed thin films of **DPP1012** (a-c), **DPP1012-4Cl** (d-f), **DPP1012-4F** (g-i) and **DPP68-4F** (j-l). Thermal annealing was carried out for 10 minutes at 200, 120, 90 and 150 °C for **DPP1012**, **DPP1012-4Cl**, **DPP1012-4F** and **DPP68-4F**, respectively, and all devices were measured in air. Insets of (a), (d), (g) and (j) show the mobility reliability factors (r).

Table S2. OTFT device performance of four molecules at different annealing temperature. The devices were measured under nitrogen.

Materials	T _{anneal} (°C)	$\mu_{e,avg} (\mu_{e,max}) [cm^2 V^{-1} s^{-1}]$	V _T (V)	I _{on} /I _{off}
DPP1012	as cast	0.11±0.04 (0.17)	-0.67±3.05	10 ³ -10 ⁴
	90	0.16±0.01 (0.17)	22.25±2.06	10 ³ -10 ⁴
	120	0.24±0.05 (0.35)	33.67±3.21	10 ³ -10 ⁴
	150	0.27±0.06 (0.35)	19.02±3.52	10 ³ -10 ⁴
	180	0.26±0.03 (0.31)	18.83±3.49	10 ⁴ -10 ⁵
	200	0.31±0.12 (0.44)	3.02±2.97	10 ⁴ -10 ⁵
DPP1012-4Cl	as cast	0.16±0.03 (0.19)	-3.75±0.96	10 ⁴ -10 ⁵
	90	0.12±0.01 (0.14)	-2.25±0.63	10 ³ -10 ⁴
	120	0.15±0.04 (0.26)	5.07±3.24	10 ³ -10 ⁴
	150	0.17±0.04 (0.24)	4.40±3.65	10 ³ -10 ⁴
	180	0.15±0.01 (0.17)	1.67±2.31	10 ² -10 ³
	200	0.13±0.04 (0.18)	-2.66±2.52	10 ³ -10 ⁴
DPP1012-4F	as cast	0.53±0.11 (0.68)	-1.20±2.86	10 ⁴ -10 ⁵
	90	0.91±0.12 (1.05)	-0.83±1.82	10 ⁴ -10 ⁵
	120	0.66±0.06 (0.76)	0.25±0.96	10 ² -10 ³
	150	0.65±0.08 (0.81)	1.67±0.51	10 ² -10 ⁴
	180	0.43±0.11 (0.57)	-7.60±2.41	10 ³ -10 ⁴
	200	0.38±0.04 (0.43)	-0.50±2.64	10 ⁴ -10 ⁵
DPP68-4F	as cast	0.16±0.04 (0.18)	7.33±2.04	10 ⁴ -10 ⁵
	90	0.34±0.06 (0.40)	-4.33±2.06	10 ² -10 ³
	120	0.41±0.07 (0.54)	-4.00±2.62	10 ² -10 ³
	150	0.41±0.08 (0.58)	-1.67±1.53	10 ⁴ -10 ⁵
	180	0.18±0.07 (0.26)	-6.20±2.95	10 ³ -10 ⁴
	200	0.10±0.06 (0.19)	2.80±3.02	10 ⁴ -10 ⁵

9. The molecular packing diagram in annealed films .

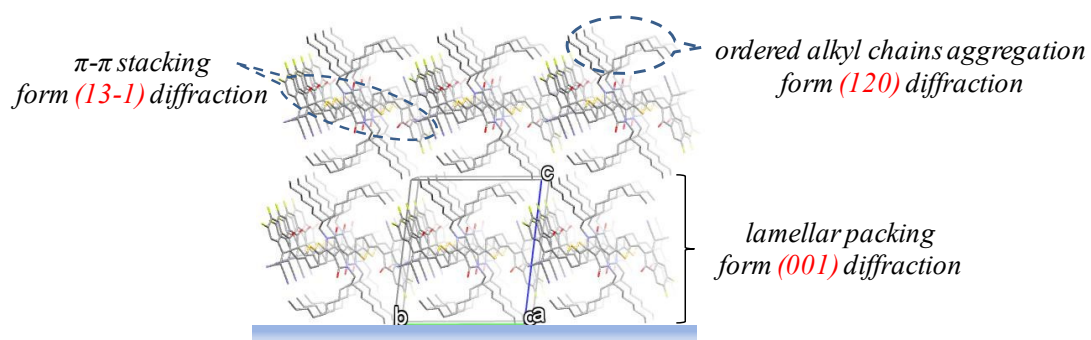


Figure S19. The molecular packing diagram in annealed films for the four compounds.

10. References

(1) P. Sonar, S. P. Singh, Y. Li, Z.-E. Ooi, T.-j. Ha, I. Wong, M. S. Soh and A. Dodabalapur.

Energy Environ. Sci. 2011, **4**, 2288-2296.

(2) T. Lei, M. Guan, J. Liu, H. C. Lin, R. Pfattner, L. Shaw, A. F. McGuire, T. C. Huang, L. Shao, K.

T. Cheng, J. B. Tok and Z. Bao, *Proc. Natl. Acad. Sci. U. S. A.* 2017, **114**, 5107-5112.